

# *Drosophila* metamorphosis involves hemocyte mediated macroendocytosis and efferocytosis

SAIKAT GHOSH<sup>#</sup>, SUSHMIT GHOSH and LOLITIKA MANDAL\*

Developmental Genetics Laboratory, Department of Biological Sciences, Indian Institute of Science Education and Research (IISER) Mohali, Knowledge City, Punjab, India

**ABSTRACT** *Drosophila* hemocytes are majorly associated with immune responses, but they also undertake several non-immune functions that are crucial during various stages of development. The activity and behaviour of hemocytes are least documented during the metamorphic phase of fly development. Here we describe the activity, form and behaviour of the most abundant type of hemocyte in *Drosophila melanogaster*, the “plasmatocyte,” throughout pupal development. Our study reveals different forms of plasmatocytes laden with varying degrees of histolyzing debris (muscle and fat) which extend beyond the size of the cell itself, highlighting the phagocytic capacity of these plasmatocytes. Interestingly, the engulfment of apoptotic debris by plasmatocytes is an actin-dependent process, and by the end of metamorphosis, clearance is achieved. The uptake of apoptotic debris consisting of muscles and lipids by the plasmatocytes provides us a model that can be employed to dissect out the relevant components of macroendocytosis and lipid-loaded phagocytosis. This understanding, by itself, is crucial for addressing the emerging role of phagocytes in physiology and pathophysiology.

**KEY WORDS:** *Drosophila*, hemocyte, efferocytosis, plasmatocyte, pupa

## Introduction

*Drosophila* hemocytes have emerged as one of the most suitable models for studying blood cell development, as a multitude of evidence state high level of conservation in form, function, and development of hemocytes to that found in higher animals (Wood and Martin, 2017). The phagocytes found in *Drosophila* are referred to as “plasmatocytes”. In addition to their role in phagocytosis (Ghosh *et al.*, 2015; Melcarne *et al.*, 2019), several studies also attribute diverse functions to plasmatocytes like wound healing (Martin and Nunan, 2015, Thuma *et al.*, 2018) and production of antimicrobial peptides (Wood and Jacinto, 2007, Vlisidou and Wood, 2015, Wang *et al.*, 2014) throughout the life cycle of *Drosophila*. Plasmatocytes, during embryogenesis, scavenge the apoptotic cells and secrete extracellular matrix proteins (ECM) for tissue morphogenesis like ventral nerve cord and renal tubule development (Bunt *et al.*, 2010, Evans *et al.*, 2010). Post-embryonically, these hemocytes rapidly divide and populate the larval hemolymph as well as some specific immunological sites present in the larval cuticle (Makhijani *et al.*,

2017, Makhijani *et al.*, 2011, Markus *et al.*, 2009). During larval stages, the plasmatocytes from embryonic origin provide necessary immunological surveillance against various pathogens like bacteria, viruses, PAMPs and also offer continuous monitoring against parasitoid wasp infection (Sorrentino *et al.*, 2002). A parallel source of larval hemocytes also arises in *Drosophila* during late embryonic stages forming a tissue of developing blood cells called the “lymph gland”, which ruptures and releases a huge number of hemocytes (majorly plasmatocytes) at the time of pupation

*Abbreviations used in this paper:* AO, acridine orange; APF, after pupal formation; Atg8, autophagy-related protein 8; CD36, cluster of differentiation 36; DEOM, dorsal exterior oblique muscle; Dia, diaphenous; DIOM, dorsal interior oblique muscle; ECM, extracellular matrix; Hml, hemolactin; LAPosome, LC3 associated protein engaged phagosome; LC3, microtubule-associated proteins 1A/1B light chain 3B; PAMP, pathogen-associated molecular pattern; R4, a fat-body specific enhancer; Rac1, Rho family of small guanosine triphosphatases; WASP, Wiskott-Aldrich syndrome protein; ZASP, Z band alternatively spliced PDZ-motif protein 52.

\*Address correspondence to: Lolitika Mandal, Developmental Genetics Laboratory, Department of Biological Sciences, Indian Institute of Science Education and Research (IISER) Mohali, Knowledge City, Sector 81, P.O. Manauli, Punjab, 140306, India. Tel: +91 172 2293172. Fax: +91 172 2240266. E-mail: lolitika@iisermohali.ac.in  
 <https://orcid.org/0000-0002-7711-6090> - #Current Address: Eunice Kennedy Shriver National Institute of Child Health and Human development (NICHD) National Institute of Health (NIH) Bethesda, MD 20892-3758, USA.

**Supplementary Material** (3 movies and 3 figures) or this paper is available at: <https://doi.org/10.1387/ijdb.190215lm>

Submitted: 18 July, 2019; Accepted: 13 August, 2019

(Grigorian *et al.*, 2011, Jung *et al.*, 2005, Lebestky *et al.*, 2000). Several *ex-vivo* approaches have demonstrated that pupal hemocytes undergo an ecdysone-dependent polarization at pre-pupal stages which not only changes their shape and behavior in real-time but also induces cytoskeletal rearrangements, leading to alteration in morphology, and motility (Moreira *et al.*, 2013, Regan *et al.*, 2013, Sampson *et al.*, 2013, Sampson and Williams, 2012, Sander *et al.*, 2013). However, previous reports did not dwell towards the later hours of pupal development and did not address the interaction of plasmatocyte with other tissues, thereby leaving the relevance of motility, and activity of plasmatocytes during pupation as an open-ended question.

Additionally, only a few studies report pieces of evidence for muscle-based debris being found within pupal hemocytes (Regan *et al.*, 2013). In this study, we have employed the whole mount *in vivo* live imaging techniques and fly genetics to analyze tremendous changes in morphology and behaviour of plasmatocytes during the entire span of *Drosophila* metamorphosis at cellular resolution. Utilizing live imaging and whole mount analysis, we have scanned the plasmatocytes throughout the pupal stages to track their activity. Our effort demonstrated their developmental role in scavenging of apoptotic debris. The significant proportion scavenged being muscle sarcolytes and a minor portion comprising of lipid droplets, making the pupal plasmatocytes as a good model for studying “macroendocytosis” (phagocytic engulfment of huge cargo) and “efferocytosis” (defined as phagocytic removal of dead/dying cells). We also report that the changes observed in the morphology and motility of plasmatocytes are an actin-dependent process. Altogether, our study reveals the developmental role of plasmatocytes in engulfing massive apoptotic bodies, especially muscle sarcolytes and immiscible lipid droplets generated actively during the histolyzing milieu of metamorphosis pupae.

## Results

### **Plasmatocytes undergo extensive changes during metamorphosis**

The activity of *Drosophila* hemocytes throughout the pupal stage is quite elusive and very less characterized. To examine the activity of plasmatocytes during metamorphosis, we utilized high-resolution imaging to image the dorsal abdominal area of pupae of genotype: *hml-Gal4.UAS-GFP* (a driver for the entire pool of plasmatocytes in circulation). The complete span of pupation, beginning from 0 h after puparium formation (APF) to 96 h APF was documented within every 24 h interval (Fig. 1A-E and quantified in 1F and Fig. S2).

Our results suggest that at 0 h APF, these hemocytes are round in morphology (Fig. 1A).

Interestingly, after 24 h APF, the hemocyte morphology underwent a complete transition from round to a large and irregularly shaped cell loaded with multiple intracellular vesicles (Fig. 1B-D and 1F). These large vesicle laden hemocytes were observed majorly during 24 h and 48 h APF, but few persisted till 72 h APF (Fig. 1D, F). However, by 96 h APF, the hemocytes were majorly devoid of any apparent intracellular vesicles and were flattened in their morphology with lamellipodial extensions (Fig. 1E).

For further characterization, we focused our analysis at 24 h APF, as during this stage, the pupae have already experienced a significant physiological change (prepupal-pupal transition). Also, at this time point, extensive tissue remodeling is an on-going process, and a

major transformation in plasmatocyte morphology and motility can be very well appreciated. Firstly, we characterized the plasmatocytes mainly based on the size of their intracellular vesicles (Fig. 1G-M). Based on our results we categorized our observed cell types into three groups: 1) small vesicle laden cells (vesicle diameter < 1  $\mu\text{m}$ ), medium vesicle laden cells (vesicle diameter ranges from 1-5  $\mu\text{m}$ ) and large vesicle laden cells (vesicle diameter  $\geq 5 \mu\text{m}$ ). Interestingly we observed that during this hour of development, large intracellular vesicles laden plasmatocytes ( $\geq 5 \mu\text{m}$ ) were the most abundant type, compared to the rest (Fig. 1N).

Careful analysis at 24 h APF also revealed the presence of a few small *hml*/GFP+ plasmatocytes (lacking large intracellular vesicles) along with the ones that are laden with multiple large vesicles (arrow in Fig. 1K). Small plasmatocytes encountered at this hour represent only 10% of the cells present in a given area, compared to the number of huge plasmatocytes (with large intracellular vesicles) (Fig. 1I,N). From this observation, we can infer that by 24 h APF, not all plasmatocytes accumulate large intracellular vesicles in them. These two types of plasmatocytes completely differed in their cellular architecture, which prompted us to analyze their movement in real time.

We next characterized these plasmatocytes based on their motility at 24 h APF. Four different motile behavior parameters were analyzed: distance traveled, velocity, turning angle, and directionality (Table 1). The motile behavior of each cell type was analyzed by measuring their cellular trajectories (Fig. 1O-P). It was quite evident that the cells without intracellular vesicles migrated a longer distance over unit time (Fig. 1P), compared to the cells with large intracellular vesicles (Fig. 1O).

Overall, we found that the total distance traveled by the small cells was more compared to plasmatocytes with large intracellular vesicles. The difference in velocity of the above plasmatocytes can be appreciated by generating a velocity heat map using four representative cells from each group (Fig. 1O-P). The color-coded ‘velocity scale’ denotes high velocity as red and lower one as blue indicating that the small cells migrated with higher velocity (Supplementary figure S1 E-H) compared to the larger ones (Supplementary figure S1A-D). Moreover, the small cells also showed the maximum ‘turning angle’, which reflects their capacity to change directions during their path of migration. In terms of ‘directionality’ which represents how direct a cell is moving towards a target, we found that although the plasmatocytes differed in their migration velocity and agility, both demonstrated random multidirectional migratory movement (Table 1). This observation suggests that during metamorphosis, plasmatocytes present in the dorsal abdomen are majorly engaged in exploring the milieu.

Thus, these vesicle laden phagocytes show different kinetic behaviour, the large one being bulky possibly by engulfment of huge histolyzed debris, hence is observed to be less motile. While the smaller ones being highly motile shows an exploratory behaviour most likely towards uncaptured debris which is continually getting histolyzed during the remodeling phase of metamorphosis. Another possibility for the slow movement of the vesicle laden hemocytes may be because of the F-actin dynamics here is reinvested to manage the movement of ingested material inside the cell.

### **Plasmatocytes accumulate large intracellular vesicles during pre-pupal to pupal transition**

To pinpoint the exact temporal window of plasmatocyte initiating the engulfment process of these huge vesicles during pupation,

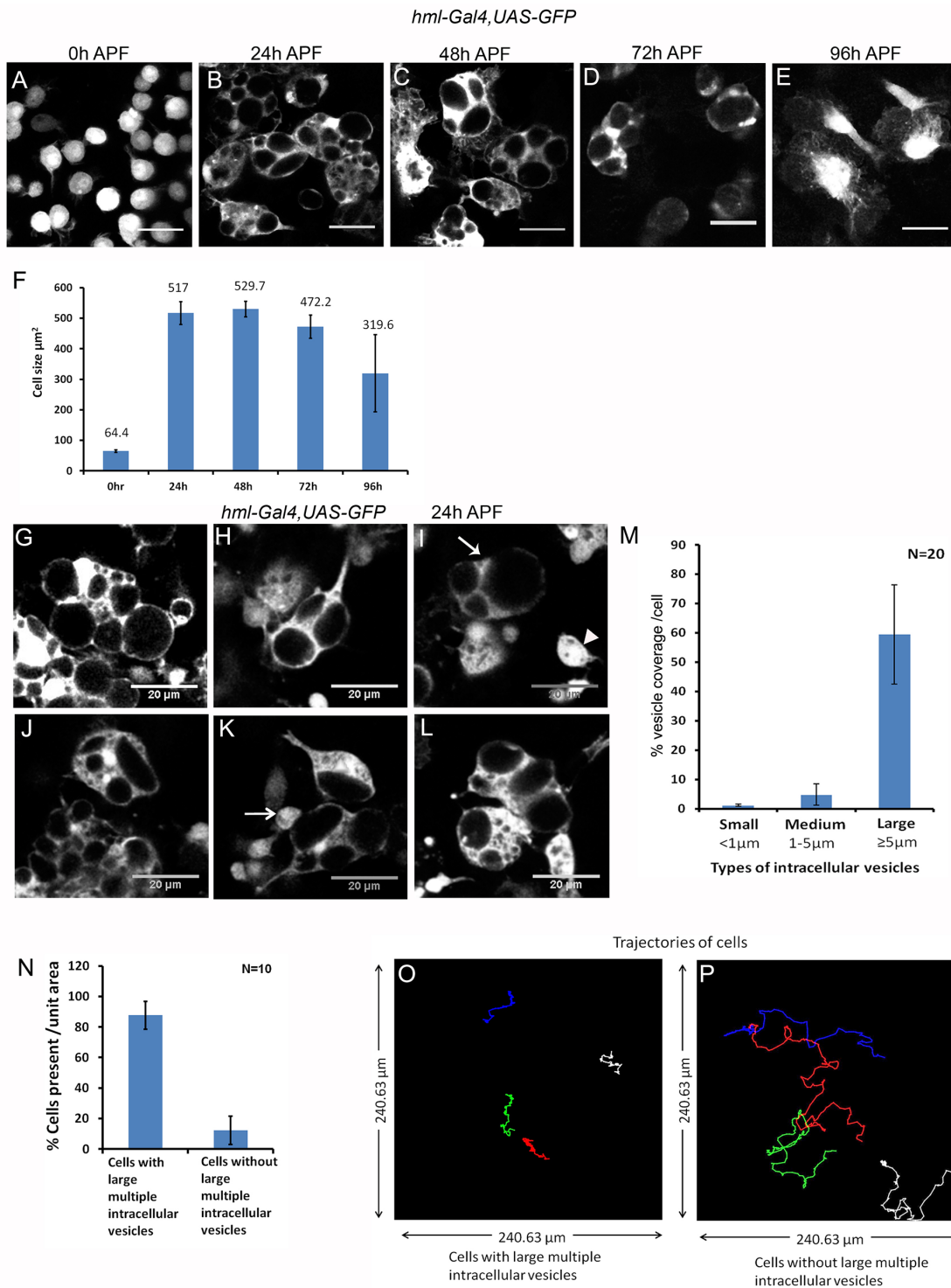


**Fig. 1. Plasmatocyte morphology and behaviour change at different stages of metamorphosis.** (A) At 0h after puparium formation (APF), plasmatocytes (visualized by *hml-Gal4>UASGFP*) change their morphology from small and round to (B) large intracellular vesicles containing plasmatocytes by 24 h APF. This change in morphology of plasmatocytes can be seen 48 h APF (C) and 72 h APF (D) as well. (E) At a later stage of pupation, the large intracellular vesicles disappear and the plasmatocytes seem flattened in their morphology. (F) The graph shows the plasmatocyte cell size at different time windows (N=10 no. of cells considered for each time point, the error bars represent Standard deviation (SD)). (G-L) 24 h APF, plasmatocytes show intracellular vesicles of different size and shape. (M) The graph shows the distribution of different types of intracellular vesicles (based on size) in pupal plasmatocytes. (N) Distribution of two different kinds of cells: 1. with large multiple intracellular vesicle containing cells (bulky: arrow at I) and 2. Cells without large multiple intracellular vesicles (small: arrowhead at I). (O,P) The trajectories bulky (O) and small (P) plasmatocytes show completely different migratory behaviour. Four colours are representing trajectories of randomly selected plasmatocytes. Scale bar, 20 µm.

we performed a more resolved temporal analysis within a narrow imaging window of two-hour intervals from 0 h APF to 12 h APF (Fig. 2 A-G). Earlier studies have revealed that at 12 h APF, a small titer of ecdysone facilitates the transition of pre-pupa to the pupal stage (Handler, 1982; Sliter and Gilbert, 1992), that generates a large amount of debris in the surrounding extracellular space.

During this analysis, we figured that these hemocytes initially transitioned from circular to an elongated morphology accompanied by filopodial extensions, which was previously described as the initial stage of polarization (Fig. 2 B-C) (Sampson *et al.*, 2013, Sampson and Williams, 2012). Further polarization of the plasmatocytes generates large lamellipodia around the cell body seen till 8 h APF. Our analyses reveal that at 12 h APF, a drastic transition of these elongated polarized cells to large size plasmatocytes loaded with intracellular cargo could be appreciated (Fig. 2G). Next, it was imperative to know how the plasmatocytes acquire large intracellular vesicles. To understand this process, we first employed light-sheet microscopy to analyze the behaviour of the actively migrating pupal phagocytes at 24 h APF (Fig. 2H-H9). The time-lapse recording revealed that in addition to constantly throwing long multi-directional filopodia, these plasmatocytes also extend lamellipodia in the surrounding space to scan the neighbourhood. We could capture instances of macroendocytosis where a cell, while undergoing migration abruptly halted and formed a large endocytic cup to engulf a hefty cargo from surrounding space (Fig. 2H-H9 and Supplementary Movie 1). Slow moving phagocytes laden with several large vesicles also extended long pseudopodia to scan the vicinity (Fig. 2 I-I9 and Supplementary Movie 2). As evident from time-lapse recording, once the phagocyte encounters the cargo, the tip of the pseudopod eventually forms an endocytic cup around the 'cargo' to engulf it. Subsequently, the engulfed cargo is dragged inside the cell body. Live imaging data also establishes that these intracellular vesicles observed at 24 h APF, are generated due to endocytosis of large multiple extracellular contents.

### Macroendocytosis by plasmatocytes is an actin dependent process

Endocytic pathways are classified into different categories depending on the size of cargo engulfed and the associated proteins involved during the process (Mayor and Pagano, 2007). In general, the endocytic pathways like clathrin-dependent, caveolin-dependent and clathrin and caveolin-independent endocytosis are involved

in a smaller size ( $< 1 \mu\text{m}$ ) cellular intake whereas phagocytosis is a process which describes the engulfment of larger cargoes up to 1-2  $\mu\text{m}$  in diameter (Mayor and Pagano, 2007). However, endocytosis of even bigger cargo size is preferably termed as macro-endocytosis (Swanson, 2008). In the current study, based on the size of the endocytic vesicles acquired by the pupal plasmatocytes (Fig. 1 G-L and Fig. 2 H-H9), along with their active membrane ruffling behavior, we infer this phagocytosis process as "macroendocytosis".

Macroendocytosis is a process heavily dependent on dynamic actin cytoskeleton rearrangement to form large endocytic cups at the site of membrane ruffling (Swanson, 2008). If indeed actin is the major component responsible for engulfment of this large apoptotic debris, then disrupting the actin cytoskeleton should drastically affect the macro-endosome formation inside the phagocyte. To test this hypothesis, the key players of actin cytoskeleton rearrangement that are known to regulate the endocytic cup formation such as Rac 1, WASP, SCAR, Diaphanous (Dia) (Swanson, 2008) were selectively down-regulated in plasmatocytes specifically, and the effect on macro-endosome formation was assayed in each genotype at 24 h APF. Compared to control, in all the above cases, phagocytes failed to accumulate macro-endosome and were unable to attain their characteristic size (Compare Fig. 2 J-J" with Fig. 2 K-O" and quantitative analysis in Fig. 2P).

Above results endorse that plasmatocytes acquire large intracellular vesicles by engulfment of several large cargoes from the extracellular environment by macro-endocytosis in actin-dependent manner.

### Pupal phagocytes recognize and engulf dying muscle debris

The two significant events that occur during the transition of pre-pupa to pupa (Handler, 1982; Sliter and Gilbert, 1992) are larval muscle histolysis and fat-body remodeling. Both of these are capable of producing large apoptotic cargoes that demand plasmatocyte mediated clearance. The first event is the histolysis of a specific group of dorsal abdominal muscles present in each segment. The dorsal abdominal muscles are divided into two groups according to their morphology and position: Dorsal External Oblique Muscle (DEOM) and Dorsal Internal Oblique Muscle (DIOM) (Wasser *et al.*, 2007). During pre-pupal to pupal transition, only DEOM undergo an ecdysone-dependent histolysis (Wasser *et al.*, 2007, Zirin *et al.*, 2013). Incidentally, the histolysis of DEOM happens within 12 h APF and produces a pool of large apoptotic muscle debris known as sarcoytes (Kuleesha *et al.*, 2016). Interestingly, how this DEOM generated pool of apoptotic sarcoytes gets cleared from the pupal system remains to be elucidated.

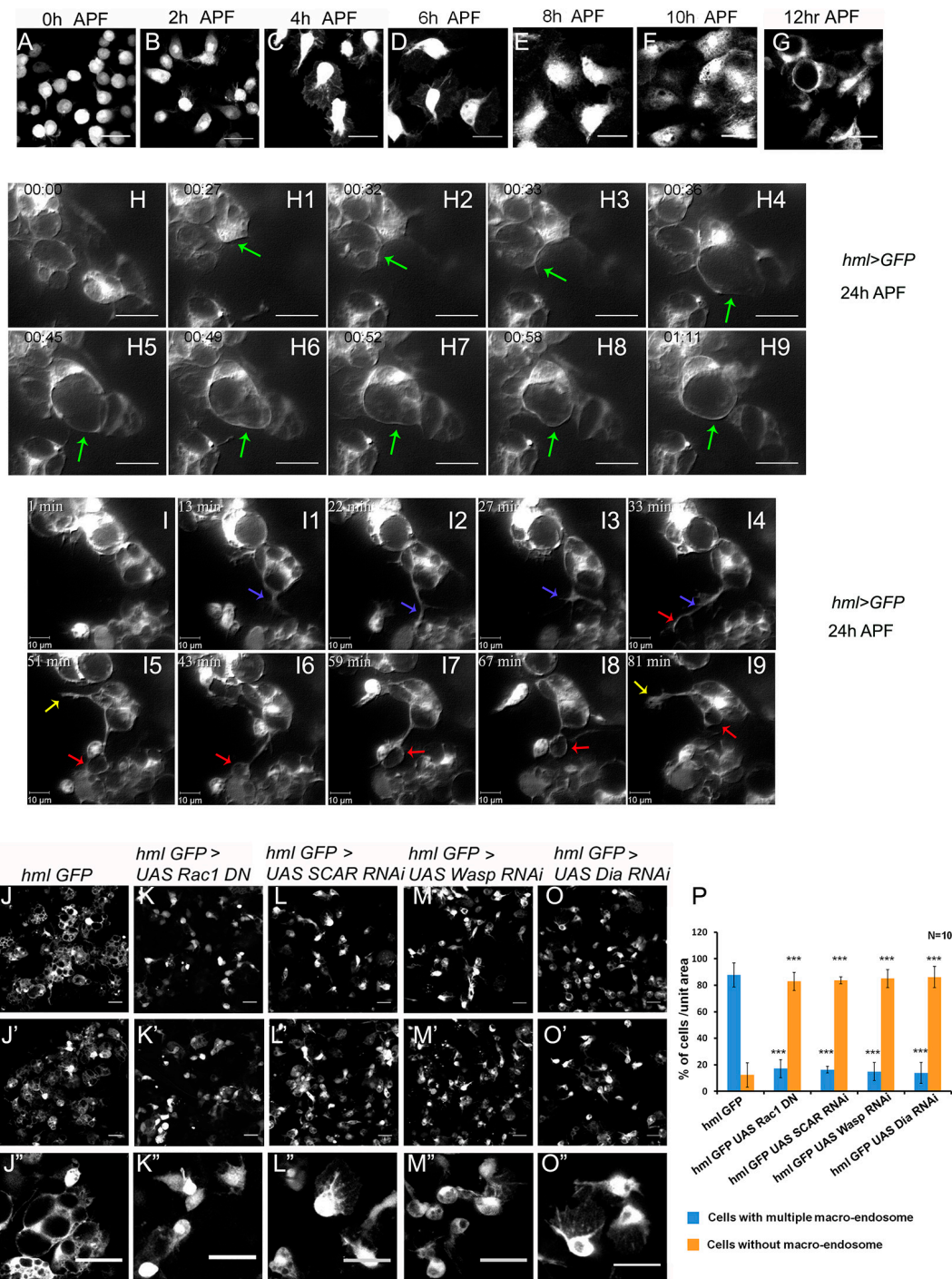
To investigate whether plasmatocytes actively participate in the clearing of sarcoytes post 12 hrs of pupation, we took synchronized pupae in which both muscles and plasmatocytes are marked (muscles visualized by GFP tagged to Z band alternatively spliced PDZ-motif protein *Zasp* (Jani and Schock, 2007) and plasmatocytes by *HmlΔ-DsRed* (Makhijani *et al.*, 2011), (Fig. 3A-A"). A long-term time-lapse recording of a pupa of this genotype was carried out from 0 h APF to 7 h APF (Fig. 3B-E"). With the onset of pupation (0 h APF), all the dorsal abdominal muscles were intact, and hemocytes were mostly present on dorsal sessile patches at the center of the abdomen. As development progresses (2 h - 4 h APF), the DEOM underwent gradual apoptosis, whereas DIOM, which is located basally, remains unaffected (Supplementary Movie

TABLE 1

#### DETAILED COMPARISON OF THE MIGRATORY BEHAVIOUR OF HEMOCYTES WITH OR WITHOUT INTRACELLULAR VESICLES

Migratory behaviours (N=25)	Cells with large multiple intracellular vesicles	Cells without large multiple intracellular vesicles
Distance travelled	113.3 $\mu\text{m}/2 \text{ h}$ (SD $\pm 13.3$ )	377.4 $\mu\text{m}/2 \text{ h}$ (SD $\pm 30.2$ )
Mean velocity	0.23 $\mu\text{m}/\text{sec}$ (SD $\pm 0.12$ )	0.78 $\mu\text{m}/\text{sec}$ (SD $\pm 0.21$ )
Maximum velocity	2.1 $\mu\text{m}/\text{sec}$ (SD $\pm 1.12$ )	4.3 $\mu\text{m}/\text{sec}$ (SD $\pm 1.5$ )
Angle of turn	100° (60° - 131°)	160° (133° - 172°)
Directionality	0.23 (SD $\pm 0.06$ )	0.24 (SD $\pm 0.08$ )

The migratory behaviour of the cells were analysed from the two hour long movie captured by time lapse images using lightsheet microscopy at 24 h APF. The time-lapse images were acquired following the image parameters: 240 time frame were acquired with a time interval of 30 secs, in a combination of 120 Z stacks of Z steps 0.457  $\mu\text{m}$ . Four migratory behaviour were analyzed: distance traveled, velocity, turning angle and directionality.



**Fig. 2. Live imaging reveals pupal plasmatocytes engulf large cargo from surrounding space via actin-dependent macroendocytosis. (A-G)** Temporal analyses (from 0-12 h APF) reveals a gradual change in plasmatocyte morphology from round shape (A) to one that are flattened with extended lamellipodia (C-D). (G) Plasmatocytes with large intracellular vesicles are evident from 12 h APF onwards. Scale bar, 20  $\mu$ m. **(H-H9)** Live imaging employing Light Sheet microscopy of pupal plasmatocyte demonstrates an engulfment of a cargo of  $\sim$ 20  $\mu$ m in diameter from surrounding space via macro-endocytosis. Green arrows indicate the formation of an endocytic cup in a plasmatocyte. Scale bar, 20  $\mu$ m. See also Supplementary Movie 1. **(I-I9)** Live imaging employing Light Sheet microscopy reveals the sequence that a bulky plasmatocyte with large intracellular vesicles employs to extend pseudopodia in order to phagocytose cargo of 5  $\mu$ m in diameter. Blue arrow marks the formation of pseudopodia. The red arrow marks the endocytic cup formed at the tip of pseudopodia. The yellow arrow marks another pseudopodia formation occurring simultaneously. Scale bar, 10  $\mu$ m. See also Supplementary Movie 2. **(J-O'')** Hemocyte specific inhibition of Rac1 using UAS-Rac1DN results in plasmatocytes which are smaller and lack large macro-endocytic vesicles compared to control (J-J'') of similar age. **(K-O'')** A similar phenotype is observed upon downregulation of SCAR, Wasp, and Dia from pupal plasmatocytes. Scale bar, 20  $\mu$ m. **(P)** The graph shows the quantification of the cells (large and small size cells) present in each genotype. P-values for Rac1=2.86X10<sup>-12</sup>, SCAR=1.09329X10<sup>-10</sup>, Wasp= 3.97791X10<sup>-13</sup>, Dia=2.731X 10<sup>-13</sup>).

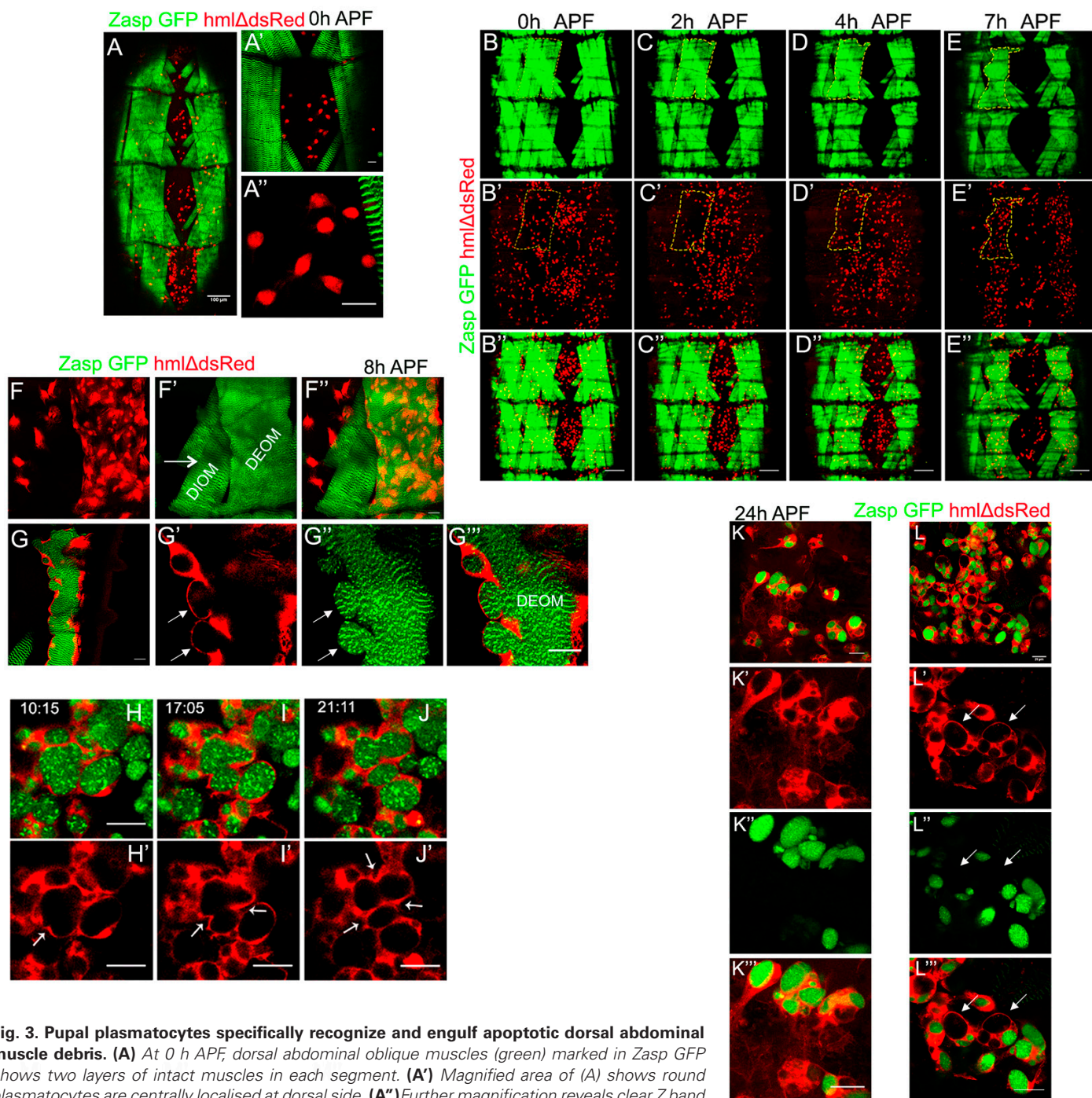


**Fig. 3. Pupal plasmatocytes specifically recognize and engulf apoptotic dorsal abdominal muscle debris.** (A) At 0 h APF, dorsal abdominal oblique muscles (green) marked in *Zasp GFP* shows two layers of intact muscles in each segment. (A') Magnified area of (A) shows round plasmatocytes are centrally localised at dorsal side. (A'') Further magnification reveals clear Z band of intact oblique muscles and plasmatocytes that are round in morphology. Scale bar, 100  $\mu$ m (A) and 20  $\mu$ m (A', A''). (B-E'') Live imaging from 0 h APF–7 h APF reveals that DEOM (Dorsal External Oblique Muscle, arrow) undergoes apoptosis which is evident by progressive constriction of muscle layer (marked in dotted line) from 4–7 h APF (D,E). (B'–D'') During DEOM histolysis, the centrally localised plasmatocytes (at 0 h APF, B', B'') undergo directed migration towards the apoptotic DEOM (E', E''). At 7 h APF majority of plasmatocytes has recognized the dying DEOM and populated the area. Scale bar, 100  $\mu$ m. See also Supplementary Movie 3. (F–F'') Plasmatocytes (red) specifically recognise and encase the entire dying DEOM layer (green) whereas DIOM (Dorsal Internal Oblique Muscle, arrow) is totally devoid of plasmatocytes. (G) A thin confocal section of the above DEOM shows plasmatocytes are not only attached to the surface but also actively engulfing from the surface of DEOM. (G'–G'') Higher magnification of G shows plasmatocytes are invading their cell membrane to engulf the apoptotic muscle (arrow). A complete engulfment of muscle sarcolepte is marked by arrowhead. Scale bar, 20  $\mu$ m. (H–J') At 12 h APF, live imaging reveals that the DEOM completely disintegrates and form sarcoleptes of different sizes (green). Plasmatocytes (red) introduce their macroendocytic cups (arrow) inside the bigger apoptotic sarcolepte (green) and thereby fragmenting them into smaller pieces for easy engulfment. Scale bar, 20  $\mu$ m. Time indicated in minutes. (K–K'') At 24 h APF, all the disintegrated large sarcoleptes (green) are engulfed by pupal plasmatocytes. (L–L'') Few plasmatocytes show macro-endosomes without apoptotic muscle content (arrow). Scale bar, 20  $\mu$ m.

3). Precisely at this time point, the hemocytes start dispersing from the central region to the dying DEOM (Compare Fig. 3B'' with 3E'' and Supplementary Movie 3). At 8 h APF, the apoptosis of DEOM was evident by overall condensation and distortion of DEOM muscle layer compare to normal morphology of the underlying DIOM (Fig. 3 F-F''). Majority of plasmatocytes were recruited to the apoptotic abdominal DEOM layer. This directed migration of the plasmatocytes become evident when the time-lapse imaging and cell tracking of the migrating hemocytes are considered together (Supplementary Movie 3 and Fig. S3 A-C). The color codes represent different time point during the journey of the migrating cells. For example blue in 'time index' represents initial time (0 h APF) where hemocytes were located majorly at the center while red indicates the final destination of hemocytes (around 7 h APF), whereby they are recruited to the dying DEOM (Supp. Fig. S3).

Time-lapse imaging also implies that the plasmatocytes possibly been receiving cues from dying DEOM that led to their directed migration and subsequent recognition of apoptotic muscle layer. Interestingly, at 8 h APF, a closer analysis of this apoptotic DEOM along with its 3D reconstruction revealed that the plasmatocytes completely encase the entire surface of dying DEOM, in contrast to the persisting DIOM (arrow) which lacked any plasmatocytes (Fig. 3F-F''). Single cell-level analysis at 8 h APF revealed that

the plasmatocytes present on the surface of the apoptotic DEOM had initiated the process of engulfing the apoptotic muscle (Fig. 3 G-G''). Time-lapse imaging of 12 h APF reveals that sarcolytes can be enclosed by more than one plasmatocytes. It also can be inferred from the observations that plasmatocytes through membrane invagination facilitate fragmentation of the large sarcolyte into smaller fragments before engulfing them (Fig. 3 H-J'). By 24 h APF, the DEOM is completely disintegrated into muscle sarcolytes of different sizes (visualized by Zasp GFP). Interestingly, none of the sarcolytes were freely present in the extracellular environment; instead, they all were engulfed by the plasmatocytes (Fig. 3K-K''). Notably, in few plasmatocytes, along with *ZaspGFP* positive intracellular vesicles few non-GFP vesicles could be seen (Fig. 3 L-L'', arrows). The above observation raised the possibility of heterogeneous endocytic cargo being engulfed by these pupal phagocytes.

In summary, these set of results help us to speculate that the dying muscles (DEOM) might be generating 'find me' signals like any other apoptotic cells (Ravichandran and Lorenz, 2007). The organized process of apoptotic cell clearance by macrophage is termed as "efferocytosis" where a specific progressive step of recruitment, recognition, and engulfment of dying cells is observed (Elliott and Ravichandran, 2016, Henson, 2017).

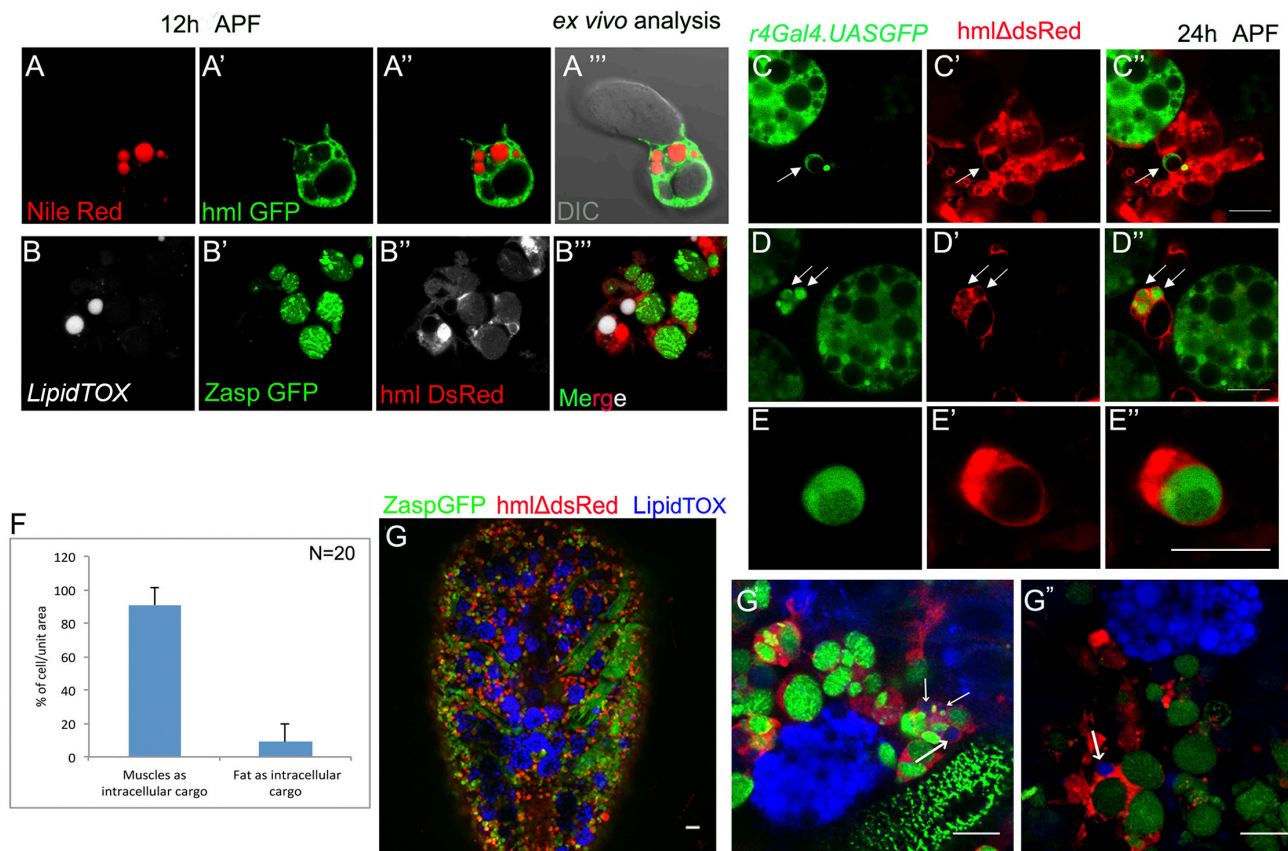


**Fig. 4. Lipids droplets are also ingested by the Pupal plasmatocytes.** (A-A'') ex vivo staining of hml GFP labelled plasmatocytes show endosomes positive for lipid droplet marked by Nile Red. DIC image reveals muscle sarcolytes (A'') engulfed along with lipid droplets by the same plasmatocyte (A-A''). (B-B'') Co-labelling of lipid (LipidTOX) and muscle (Zasp GFP) in the pupal plasmatocyte endorses the above results. Scale bar, 20 µm. (C-E'') Using genetic marker for fat body (*R4-Gal4>UAS-GFP*) several pupal plasmatocyte (*hmlDsRed*) can be seen harboring lipid droplets (arrow) which are released by remodelled fat cells. Scale bar, 20 µm. (F) Quantitative analyses of cargo content in macro-endosomes. (G-G'') In vivo evidence of lipid droplets engulfed by plasmatocytes in a pupae: Arrows point out to Plasmatocytes (red) that have ingested lipid droplets marked by LipidTOX.

Interestingly, in the current study, the pupal plasmatocytes seem to demonstrate all the steps of efferocytosis, at initial 4-7 h APF plasmatocytes disperse and accurately recognize the dying blebs of DEOM before engulfing the sarcoleptes.

**Plasmatocytes engulf lipids from fat bodies during metamorphosis**

The second significant event which occurs within the same time frame of head eversion is remodeling of larval fat-body. In response to ecdysone signaling, tightly attached larval fat layer converts into individualized, free-floating round fat cells in pupa (Nelliot et al., 2006, Zheng et al., 2016). In *Drosophila*, remodeling of the larval fat body also takes place during the initial phase (around 12 h APF) of metamorphosis, a sheet of polygonal larval fat cells dissociates into individual free floating round fat cells (Nelliot et al., 2006, Zheng et al., 2016). During metamorphosis, these fat cells release energy in the form of lipid droplets to surrounding tissues to maintain the energy requirement in the non-feeding state of pupal life (Aguila et al., 2007). The lipid droplets are made up of neutral lipids in the center, phospholipid monolayer, and lipid droplet-associated proteins (Bi et al., 2012, Brasaemle, 2007). These lipid droplets can be easily visualized by neutral lipid stains like LipidTOX or Nile red (Bi et al., 2012, Tian et al., 2011).

We next decided to probe whether these lipid droplets released by the remodeled fat cells are also present in the vesicle laden

plasmatocytes. We performed *ex-vivo* Nile red labeling (Fig. 4A-A'') in a genotype where the plasmatocytes were visualized by *hml-Gal4>UAS-GFP*. Several hemocytes were seen that had engulfed muscle sarcolepte yet had Nile red positive vesicles in them. Similar results were obtained on *ex-vivo* LipidTOX in pupal bleed of a genotype in which muscle (*Zasp GFP*), as well as plasmatocytes (*hmlΔdsRed*) were labeled (Fig. 4 B-B''). The plasmatocytes were scored based on their cargo composition: the proportion of them which engulfed fat vs. muscle was also taken into account. Since a majority of the intracellular content of these hemocytes are muscle sarcoleptes (Fig. 4F), it can thus be concluded that sarcoleptes are the major cargoes.

We also genetically marked fat cells with *r4-Gal4>UAS-GFP* (a fat body-specific driver line) and plasmatocytes marked with *hmlΔdsRed* (Fig. 4 C-E''). Results show that besides the GFP expressing globular free-floating fat cells, few plasmatocytes (marked in red) were also positive for GFP expression (Fig. 4D and D'', arrow). This GFP expression inside the intracellular vesicles of plasmatocytes suggests that the released fat contents are also ingested by these pupal hemocytes.

To further validate our *ex-vivo* analyses, we performed *in vivo* LipidTOX staining in pupae in which muscle was marked with *Zasp GFP* and hemocytes with *hmlΔdsRed*. We found a small but observable proportion of vesicle positive for LipidTOX, indicating the presence of neutral lipids inside the vesicle (arrows in Fig. 4 G-G'').

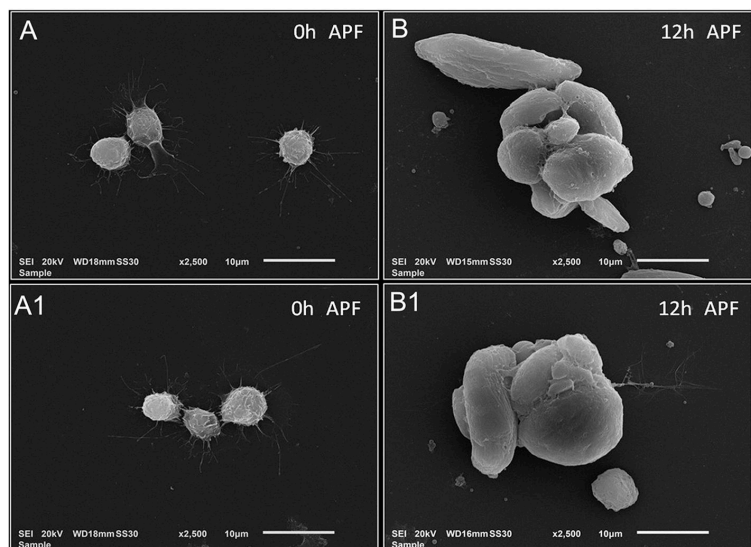
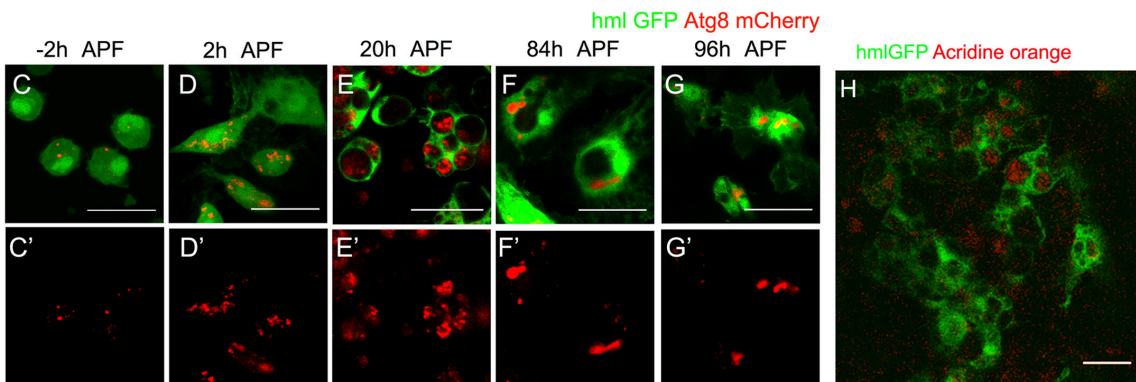


**Fig. 5. Autophagy player Atg might facilitate the process of cargo degradation.** Scanning electron micrograph of 0 h APF vs. 12 h APF pupal plasmatocytes. (A,A1) Plasmatocytes isolated from the 0h APF pupal bleed are small in size. (B,B1) At 12 h APF plasmatocyte are large in size, irregularly shaped with multiple macro-endosome. (C-D') Plasmatocytes show an increase mCherry-Atg8a expression during initial pupal development.



(E-E') At 20 h APF, the increased Atg8 expression is observed inside the macro-endosomes. (F-G') At late pupal stages, Atg8 expression declines. Scale bar, 20 µm. (H) Acridine orange injection in mid late pupae indicated lowering of pH in ingested vesicles signifying the initiation of degradation process.

Therefore, the major reason for this drastic change in plasmatocyte morphology in the pupal stage was due to phagocytosis of apoptotic debris comprising majority of sarcoyte and a small proportion of lipid droplets. The extensive alteration in the morphology of the plasmatocytes due to efferocytosis was also evident from the scanning electron micrograph of 0 h APF vs. 12 h APF pupal bleed (See Fig. 5 A-B1).

### **Apoptotic load ingested by the plasmatocytes is degraded in lysosomes**

In mammals, during apoptotic cell clearance phagocytes are recruited to the site of apoptosis, where they recognize and engulf dying cells and then destroy them in a silent immunological manner via lysosomal fusion (Henson, 2017). To examine the degradative fate of these huge ingested vesicles, we used a pH-sensitive dye, Acridine Orange (AO), which commonly labels acidic vesicle. We found that after injecting AO in the dorsal abdominal portion of a mid-late pupa, most of these vesicles were positively stained by AO, hence implying the acidification of these ingested particles is already initiated (Fig. 5H). However, very recently it was reported that autophagic protein LC3 is also incorporated into a single membrane phagosome (Green *et al.*, 2016, Martinez *et al.*, 2011), after the engulfment of an extracellular apoptotic corpse. This LC3 associated phagosome is called LAPosome (Green *et al.*, 2016), which indicative of additional evidence of a phagosomal degradation process being initiated after apoptotic corpse engulfment.

Taking a cue from these mammalian studies, we wanted to figure out the localization of LC3 homolog in fly "Atg8" and analyzed the fate of these phagosomes in a hemocyte-specific manner (*hml-Gal4, UAS-GFP, UAS-mCherry-Atg8a* fly line). Very low expression of Atg8 in the cytosol can be detected in the hemocytes around 2 hrs before pupa formation (Fig. 5C). However, by 20 h APF, the expression of Atg8 becomes reasonably high (Fig. 5 E-E') compared to the early pupal stages (Fig. 5 C-D'). Surprisingly, this strong expression of mcherry-Atg8a was restricted to the large macroendocytic vesicles instead of the cytosol, which suggests that autophagy protein Atg8 was attached to these large phagosomes. At 84 h APF, the remaining intracellular vesicles were devoid of Atg8 expression instead Atg8 was present separately in the cytoplasm (Fig. 5 F-F'). In late 96 h APF, when plasmatocytes regain their normal morphology after digesting the intracellular cargoes, the mcherry-Atg8a expression not only decreases but gets re-localized to the cytoplasm (Fig 5 G-G'). Therefore, Atg8 localization study demonstrated a dynamic change in the distribution and levels of Atg8 with respect to different developmental stages of pupal plasmatocytes involved in the clearance of apoptotic muscles. Based on these results, we infer that this ingested apoptotic debris undergoes an acidic degradation through a LAPosome like vesicle.

### **Conclusion**

Plasmatocytes lineage has been known to show a lot of parallels to that of a monocyte-macrophage lineage (Wood 2007). Plasmatocytes just like a vertebrate macrophage harbours a vast array of scavenger receptors including the members of the CD36 family, which are extensively involved in apoptotic corpse engulfment along with receptors like draper responsible for recognizing "eat me" signal provided by apoptotic corpses (Manaka 2004). Our study reports the presence of two different kinds of vesicles

being present in pupal plasmatocytes, one containing huge muscle sarcoytes and the other houses few lipid droplets, making plasmatocytes a rather complicated and multi-dimensional phagocyte.

Altogether, we provide extensive developmental insights into plasmatocyte activity during pupal stages and its ability to engulf and scavenge apoptotic muscle and lipid debris. We further propose that these engulfed debris experience a highly acidic/degradative environment within the vesicle. Along with that, the vesicles also harbours similar machinery, which is observed during LC3 based phagosome formation during efferocytosis within vertebrate macrophages (Green *et al.*, 2016). Thus, this finding makes *Drosophila* plasmatocytes an attractive model for studying apoptotic clearance and interactions between phagocytic and autophagic machinery of macrophages.

### **Materials and Methods**

#### **Fly genetics**

*hml-Gal4, UAS-2xEGFP* (BDSC#30140), *ZaspGFP* (BDSC#6838), *R4-Gal4* (BDSC#33832), *UAS-mCherry-Atg8a* (BDSC#37750), *UAS-Rac1DN* (BDSC#6296), *UAS-Wasp RNAi* (BDSC#25955), *UAS-SCAR RNAi* (BDSC#31126), *UAS-Dia RNAi* (VDRC#103914) flies were obtained from Bloomington *Drosophila* Stock Center (BDSC) and Vienna *Drosophila* Resource Centre (VDRC). *hml ΔDsRed* (Katja Bruckner, UCSF, USA) was a kind gift from U Banerjee.

#### **Live imaging of pupa**

Synchronized white prepupae were selected and cultured until the required stage. Till 14 h APF, imaging of pupae (0, 12 and 14 h) was done directly. However, for all the stages depicted beyond 14 h APF (like the stages of 24, 48, 27 and 96 h APF), care was taken to remove the inert brown outer cuticle (also termed as the pupal case) before imaging following a standard protocol (Sander *et al.*, 2013). The pupae were placed in a small drop of Halocarbon oil 700 (Sigma) with the dorsal side down so that the abdomen was directly visible through cover-slip for imaging. The activities of fluorescently marked pupal hemocytes were recorded in confocal microscope through time-lapse imaging. Images were taken generally on the lateral side of dorsal abdominal segment A1. High speed live imaging of pupa was also carried out in Light-sheet microscope.

#### **Light sheet microscopy**

The sample preparation and the principle of light sheet microscopy was quite different from conventional confocal microscopy. In light sheet microscopy sample was put inside a capillary using 1% low melting agarose (Sigma Aldrich). The capillary containing sample was suspended inside a special chamber of light sheet microscope, which was filled with distilled water and imaged by one water dipped 20x objective lens (for acquiring emission light) and two 10X lens (for sample illumination) in a Zeiss Light Sheet Z.1 microscope. The time-lapse images were captured by the following parameters: 240-time frames were captured with an interval of 30 second, in a combination of 120 Z stacks of step size 0.467 μm. Movies were prepared at a speed of 15 frame per second (fps).

#### **Scanning electron microscopy**

For scanning electron microscopy (SEM) of 12 h APF pupal plasmatocytes, cells were collected from pupal bleed and was fixed in 6% PFA for 1 h by adding the PFA in the PBS drop containing the cells. The samples were again fixed in 2.5% Glutaraldehyde (GA) for 2 h and washed thrice in 1X PBS. The samples were subsequently processed for serial dehydration using ethanol concentration of 10%, 20%, 30%, 50%, 70%, 90%, for 15min each and finally at 100%. Samples were subjected to complete dehydration and drying with a mixture of HMDS and Ethanol (1:1), followed by 100% HMDS (Hexamethyldisilazane, Sigma) till the solu-

tion dries completely. The cover glass was gently arranged on a surface of carbon tape attached in SEM stab. Then samples were gold coated in a coater (Q150R ES, Quorum Technologies Ltd) with the run profile parameters: Material- Gold, Sputter current-50mA, Sputter time 100second and Tooling factor 5.00. Finally the gold coated samples were imaged in Jeol Scanning electron microscope (JSM-6010PLUS/LV).

#### Lipid staining of whole mount pupae

Synchronized white prepupae were selected and cultured until the required stage. The pupal covering was carefully removed, followed by fixation of whole pupae in 10% PFA for 6-12 hours in 4°C. The fixed pupae were washed with 1x PBS then incubated in 200x HCS LipidTOX™ Deep Red neutral lipid stain (Invitrogen) prepared in DMSO for 1-2 hrs at room temperature (excessive incubation may affect the morphology of the pupae), followed by two wash with plain DMSO for 10 minutes. Finally, a small drop of Halocarbon oil 700 (Sigma) was placed on cover-slip of glass bottom dish. The abdominal portion of the pupae was then mounted onto the halocarbon oil and was imaged.

#### Acridine orange Injections

The pupal case of synchronized pupae was removed carefully; these pupae were then injected with 50-100nl of 0.5mg/ml of AO (Invitrogen A1301) in the dorsal side of the abdomen using Femtojet Express pneumatic injector. These live injected pupae were then mounted with halocarbon oil over glass bottom dish and imaged within 10 mins post-injection.

#### Ex vivo pupal hemocyte isolation and staining

A drop of 20 µl 1X PBS was taken on a clean cover glass of 24mm square area. A synchronized pupa of the required stage was kept in the PBS drop. Next, using two needles, the abdomen was exposed by a fine incision without disturbing the internal structures much. The exposed region was carefully positioned in the drop of PBS for 10 seconds to collect the hemolymph along with blood cells. The bleed was collected on the cover-slip surface was immediately followed by fixation with 6% PFA for 20min in room temperature (RT). The fixative was washed with PBS twice. The fixed bleed was then labeled with neutral lipid dyes like 10uM Nile red and 10x LipidTOX for 30 minutes.

#### Imaging

Imaging was performed in Confocal microscope Zeiss LSM780, Leica SP8 and Lightsheet microscope Zeiss Z.1. Images were processed and analyzed in Fiji/Image J software.

The colour coded velocity map image of migrating cells was created using the Nikon Imaging software – NIS Elements Advance Research (AR) Version 5.02.01.

The time projection map of migrating pupal hemocytes was generated through cell tracking module of IMARIS.

#### Quantitative analysis

For quantitative analysis, graphs were prepared in Microsoft Excel software where the error bars represent Standard deviation (SD) and for the comparison, students t-test were performed to analyse statistical significance. p-values were mentioned in the corresponding legends. p-value <0.05 as \*, <0.005 as \*\* and <0.0005 as \*\*\*. All the experiments were conducted minimum thrice and in graphs N represent the number of samples analysed.

#### Acknowledgements

We thank U Banerjee for flies. We thank IISER Mohali's Confocal Facility, Bloomington Drosophila Stock Center, Indiana University, Drosophila Genomics Resource Center, Kyoto and Developmental Studies Hybridoma Bank, the University of Iowa for flies and antibodies. We thank Carl Zeiss India (Bangalore) Pvt. Ltd. for the accessibility to light sheet microscope. Special thanks to Chad Williamson, Eunice Kennedy Shriver National Institute of Child Health and Human Development (NICHD), National

Institute of Health, Bethesda, MD, USA for help with velocity heat maps. We acknowledge CSIR for funding to S.G and S.G., and Wellcome Trust DBT IA Senior Fellowship [IA/S/17/1/503100] to L.M.

#### Author contributions

Saikat Ghosh: Conceived, Designed and performed bulk of the experiments, Acquisition of data, Analysis and interpretation of data, Co-wrote the manuscript. Sushmit Ghosh: Helped with in-vivo experiments, analysis, interpretation of data and drafted the manuscript. LM Design, Analysis and interpretation of data, Co-wrote the manuscript and research supervision.

#### References

- AGUILA, J.R., SUSZKO, J., GIBBS, A.G. and HOSHIZAKI, D.K. (2007). The role of larval fat cells in adult *Drosophila melanogaster*. *J Exp Biol* 210: 956-963.
- BI, J., XIANG, Y., CHEN, H., LIU, Z., GRONKE, S., KUHNLEIN, R.P. and HUANG, X. (2012). Opposite and redundant roles of the two *Drosophila* perilipins in lipid mobilization. *J Cell Sci* 125: 3568-3577.
- BRASAEMLE, D.L. (2007). Thematic review series: adipocyte biology. The perilipin family of structural lipid droplet proteins: stabilization of lipid droplets and control of lipolysis. *J Lipid Res* 48: 2547-2559.
- BUNT, S., HOOLEY, C., HU, N., SCAHILL, C., WEAVERS, H. and SKAER, H. (2010). Hemocyte-secreted type IV collagen enhances BMP signaling to guide renal tubule morphogenesis in *Drosophila*. *Dev Cell* 19: 296-306.
- ELLIOTT, M.R. and RAVICHANDRAN, K.S. (2016). The Dynamics of Apoptotic Cell Clearance. *Dev Cell* 38: 147-160.
- EVANS, I.R., HU, N., SKAER, H. and WOOD, W. (2010). Interdependence of macrophage migration and ventral nerve cord development in *Drosophila* embryos. *Development* 137: 1625-1633.
- GHOSH, S., SINGH, A., MANDAL, S. and MANDAL, L. (2015). Active hematopoietic hubs in *Drosophila* adults generate hemocytes and contribute to immune response. *Dev Cell* 33: 478-88.
- GREEN, D.R., OGUIN, T.H. and MARTINEZ, J. (2016). The clearance of dying cells: table for two. *Cell Death Differ* 23: 915-926.
- GRIGORIAN, M., MANDAL, L. and HARTENSTEIN, V. (2011). Hematopoiesis at the onset of metamorphosis: terminal differentiation and dissociation of the *Drosophila* lymph gland. *Dev Genes Evol* 221: 121-131.
- HANDLER, A.M. (1982). Ecdysteroid titers during pupal and adult development in *Drosophila melanogaster*. *Dev Biol* 93: 73-82.
- HENSON, P.M. (2017). Cell Removal: Efferocytosis. *Annu Rev Cell Dev Biol* 33: 127-144.
- JANI, K. and SCHOCK, F. (2007). Zasp is required for the assembly of functional integrin adhesion sites. *J Cell Biol* 179: 1583-1597.
- JUNG, S.H., EVANS, C.J., UEMURA, C. and BANERJEE, U. (2005). The *Drosophila* lymph gland as a developmental model of hematopoiesis. *Development* 132: 2521-2533.
- KULEESHA, Y., PUAH, W.C. and WASSER, M. (2016). Live imaging of muscle histolysis in *Drosophila* metamorphosis. *BMC Dev Biol* 16: 12.
- LEBESTKY, T., CHANG, T., HARTENSTEIN, V. and BANERJEE, U. (2000). Specification of *Drosophila* hematopoietic lineage by conserved transcription factors. *Science* 288: 146-149.
- MAKHJANI, K., ALEXANDER, B., RAO, D., PETRAKI, S., HERBOSO, L., KUKAR, K., BATOOL, I., WACHNER, S., GOLD, K.S., WONG, C. et al., (2017). Regulation of *Drosophila* hematopoietic sites by Activin-beta from active sensory neurons. *Nat Commun* 8: 15990.
- MAKHJANI, K., ALEXANDER, B., TANAKA, T., RULIFSON, E. and BRUCKNER, K. (2011). The peripheral nervous system supports blood cell homing and survival in the *Drosophila* larva. *Development* 138: 5379-5391.
- MARKUS, R., LAURINYEZ, B., KURUCZ, E., HONTI, V., BAJUSZ, I., SIPOS, B., SOMOGYI, K., KRONHAMN, J., HULTMARK, D. and ANDO, I. (2009). Sessile hemocytes as a hematopoietic compartment in *Drosophila melanogaster*. *Proc Natl Acad Sci USA* 106: 4805-4809.
- MARTIN, P. and NUNAN, R. (2015). Cellular and molecular mechanisms of repair in acute and chronic wound healing. *Br J Dermatol* 173: 370-378.

- MARTINEZ, J., ALMENDINGER, J., OBERST, A., NESS, R., DILLON, C.P., FITZGERALD, P., HENGARTNER, M.O. and GREEN, D.R. (2011). Microtubule-associated protein 1 light chain 3 alpha (LC3)-associated phagocytosis is required for the efficient clearance of dead cells. *Proc Natl Acad Sci USA* 108: 17396-17401.
- MAYOR, S. and PAGANO, R.E. (2007). Pathways of clathrin-independent endocytosis. *Nat Rev Mol Cell Biol* 8: 603-612.
- MELCARNE, C., LEMAITRE, B. and KURANT, E. (2019). Phagocytosis in *Drosophila*: From molecules and cellular machinery to physiology. *Insect Biochem Mol Biol* 109: 1-12.
- MOREIRA, C.G., JACINTO, A. and PRAG, S. (2013). *Drosophila* integrin adhesion complexes are essential for hemocyte migration in vivo. *Biol Open* 2: 795-801.
- NELLIOT, A., BOND, N. and HOSHIZAKI, D.K. (2006). Fat-body remodeling in *Drosophila melanogaster*. *Genesis* 44: 396-400.
- REGAN, J.C., BRANDAO, A.S., LEITAO, A.B., MANTAS DIAS, A.R., SUCENA, E., JACINTO, A. and ZAIDMAN-REMY, A. (2013). Steroid hormone signaling is essential to regulate innate immune cells and fight bacterial infection in *Drosophila*. *PLoS Pathog* 9: e1003720.
- SAMPSON, C.J., AMIN, U. and COUSO, J.P. (2013). Activation of *Drosophila* hemocyte motility by the ecdysone hormone. *Biol Open* 2: 1412-1420.
- SAMPSON, C.J. and WILLIAMS, M.J. (2012). Real-time analysis of *Drosophila* post-embryonic haemocyte behaviour. *PLoS One* 7: e28783.
- SANDER, M., SQUARR, A.J., RISSE, B., JIANG, X. and BOGDAN, S. (2013). *Drosophila* pupal macrophages--a versatile tool for combined ex vivo and in vivo imaging of actin dynamics at high resolution. *Eur J Cell Biol* 92: 349-354.
- SLITER, T.J. and GILBERT, L.I. (1992). Developmental arrest and ecdysteroid deficiency resulting from mutations at the dre4 locus of *Drosophila*. *Genetics* 130: 555-68.
- SORRENTINO, R.P., CARTON, Y. and GOVIND, S. (2002). Cellular immune response to parasite infection in the *Drosophila* lymph gland is developmentally regulated. *Dev Biol* 243: 65-80.
- SWANSON, J.A. (2008). Shaping cups into phagosomes and macropinosomes. *Nat Rev Mol Cell Biol* 9: 639-649.
- THUMA, L., CARTER, D., WEAVERS, H. and MARTIN, P. (2018). *Drosophila* immune cells extravasate from vessels to wounds using Tre1 GPCR and Rho signaling. *J Cell Biol* 217: 3045-3056.
- TIAN, Y., BI, J., SHUI, G., LIU, Z., XIANG, Y., LIU, Y., WENK, M.R., YANG, H. and HUANG, X. (2011). Tissue-autonomous function of *Drosophila* seipin in preventing ectopic lipid droplet formation. *PLoS Genet* 7: e1001364.
- VLISIDOU, I. and WOOD, W. (2015). *Drosophila* blood cells and their role in immune responses. *FEBS J* 282: 1368-1382.
- WANG, L., KOUNATIDIS, I. and LIGOXYGAKIS, P. (2014). *Drosophila* as a model to study the role of blood cells in inflammation, innate immunity and cancer. *Front Cell Infect Microbiol* 3: 113.
- WASSER, M., BTE OSMAN, Z. and CHIA, W. (2007). EAST and Chromator control the destruction and remodeling of muscles during *Drosophila* metamorphosis. *Dev Biol* 307: 380-393.
- WOOD, W. and MARTIN, P. (2017). Macrophage Functions in Tissue Patterning and Disease: New Insights from the Fly. *Dev Cell* 40: 221-233.
- ZHENG, H., YANG, X. and XI, Y. (2016). Fat body remodeling and homeostasis control in *Drosophila*. *Life Sci* 167: 22-31.
- ZIRIN, J., CHENG, D., DHANYASI, N., CHO, J., DURA, J.M., VIJAYRAGHAVAN, K. and PERRIMON, N. (2013). Ecdysone signaling at metamorphosis triggers apoptosis of *Drosophila* abdominal muscles. *Dev Biol* 383: 275-284.

**Further Related Reading, published previously in the *Int. J. Dev. Biol.***

**Ontogeny of the *Drosophila* larval hematopoietic organ, hemocyte homeostasis and the dedicated cellular immune response to parasitism**

Joanna Krzemien, Michele Crozatier and Alain Vincent  
Int. J. Dev. Biol. (2010) 54: 1117-1125  
<https://doi.org/10.1387/ijdb.093053jk>

**HOX genes in normal, engineered and malignant hematopoiesis**

Emma M. Collins and Alexander Thompson  
Int. J. Dev. Biol. (2018) 62: 847-856  
<https://doi.org/10.1387/ijdb.180206at>

**Early hematopoietic and vascular development in the chick**

Hiroki Nagai, Masahiro Shin, Wei Weng, Fumie Nakazawa, Lars Martin Jakt, Cantas Alev and Guojun Sheng  
Int. J. Dev. Biol. (2018) 62: 137-144  
<https://doi.org/10.1387/ijdb.170291gs>

**Disruption of the aortic wall by coelomic lining-derived mesenchymal cells accompanies the onset of aortic hematopoiesis**

Alaa A. Arraf, Marella F.T.R. De Bruijn and Thomas M. Schultheiss  
Int. J. Dev. Biol. (2017) 61: 329-335  
<https://doi.org/10.1387/ijdb.170012ts>

**The Leo Sachs' legacy: a pioneer's journey through hematopoiesis**

Joseph Lotem and Yoram Groner  
Int. J. Dev. Biol. (2017) 61: 127-136  
<https://doi.org/10.1387/ijdb.160262yg>

**Hippo signaling components, Mst1 and Mst2, act as a switch between self-renewal and differentiation in *Xenopus* hematopoietic and endothelial progenitors**

Susumu Nejjigane, Shuji Takahashi, Yoshikazu Haramoto, Tatsuo Michiue and Makoto Asashima  
Int. J. Dev. Biol. (2013) 57: 407-414  
<https://doi.org/10.1387/ijdb.130010st>

**A novel role of the glial fate determinant glial cells missing in hematopoiesis**

Cécile Jacques, Laurent Soustelle, István Nagy, Céline Diebold and Angela Giangrande  
Int. J. Dev. Biol. (2009) 53: 1013-1022

